JOURNAL OF CATALYSIS 34, 411–422 (1974)

Supported Platinum Catalysts—Small Angle X-Ray Scattering and Chemisorption

A. RENOUPREZ, C. HOANG-VAN AND P. A. COMPAGNON

Institut de Recherches sur la Catalyse, 39 Boulevard du 11 Novembre 1918, 69100 Villeurbanne, France

Received June 26, 1973; revised January 17, 1974

The area of platinum in alumina supported catalysts was determined by chemisorption of hydrogen or carbon monoxide and small angle X-ray scattering. The agreement between the results is good enough to corroborate a hypothesis on the stoichiometry of the adsorption reaction over a wide range of particle size. The distributions in the diameter obtained by electron microscopy and small angle X-ray scattering are in good agreement when the particles are homodispersed.

INTRODUCTION

The aim of this work was to study the morphology of supported platinium catalysts by independent physical and chemisorption methods. This comparison is based on small angle X-ray scattering and chemisorption of CO and H_2 for metallic area determination and on small angle and electron microscopy for particle diameter distribution.

Recent improvements in the field of small angle X-ray scattering theory give special interest to this comparison, since up to this time application of multiple scattering mathematical treatment to a three phase system has not yet been done. In general, the use of this method has been limited to mean parameter determination and it is of interest to extend this, i.e., to determine the metallic area and diameter distribution curves and to check the results with chemisorption data.

EXPERIMENTAL METHODS

Catalysts

The support is an amorphous alumina prepared from aqueous solutions of aluminium chloride and ammonium carbonate (*1*). Some properties of this alumina have been described earlier (*2–4*). This amorphous oxide is transformed into η-alumina by heating for 15 hr at 700°C in air or 800°C *in vacuo* (*1*). Otherwise, this solid becomes an *n*-type semiconductor by heating in high vacuum (10^{-6} Torr) between 450 and 730°C or a *p*-type semiconductor at higher temperature (*2*). These treatments also produce oxidizing and reducing sites on the alumina surface, as shown by EPR (*4*). Such unusual properties of the solid have led us to use it as a carrier for supported platinum catalysts to show the possible influence of the support on the properties of the metal.

The Pt is introduced by shaking 1 g of alumina with 10 cm^3 of water containing the required amount of hexachloroplatinic acid. The sample is then dried in vacuum at 100°C for 16 hr and then reduced at 500°C in hydrogen flow for 3 hr. In doing so, the texture and amorphous state of the support are preserved (*5*). Analyses of Pt and Cl are respectively performed by colorimetry and radioactivation (*6*). All reduced samples, containing 1 to 4% Pt, retained about 0.6% Cl (*5*).

Chemisorption Measurements

The chemisorption of gases such as H_2, CO and O_2 has been extensively used for

surface area determination of metallic catalysts (*7–11*). This method is based on two main assumptions: (i) there is no chemisorption on the support and (ii) for a given metal-adsorbate pair, the reaction stoichiometry depends neither on the particle size nor on the nature of the carrier. A suitable choice of the chemisorption temperature can avoid tedious corrections for adsorption on the support. However, some authors assume that the chemisorption stoichiometry could depend on the size of metal particles. This seems to be the case for ultrafine Pt particles where a Pt surface atom can retain up to two H atoms (*12–14*). In the case of CO and O_2, examples of the variation of stoichiometry with particle size and carrier nature have been reported (*15–17*).

One of our purposes is to verify, by comparison with small angle scattering, the possible variation of the stoichiometry of CO and H_2 chemisorption on differently dispersed catalysts. These adsorbates (CO and H_2) have given results in good agreement (*18, 19*).

a. Hydrogen Chemisorption

In the general case, hydrogen chemisorption may be represented by the following equation:

$$H/Pt = H/Pt_s \times Pt_s/Pt$$

where Pt_s is the number of surface Pt atoms and Pt the total number of Pt atoms. The ratio Pt_s/Pt represents the Pt dispersion connected to the metal surface area. For this work, we have assumed that $H/Pt_s = 1$. So, the determination of the amount of chemisorbed hydrogen allows the measurement of the metal dispersion.

The volume of irreversibly adsorbed hydrogen at 200°C on Pt is measured by a pulse adsorption method which consists in a modification of that of Figueras, De Mourgues and Trambouze (*20*). In our method, the injection of a mixture of H_2–N_2 containing 5.7% H_2 (instead of pure H_2) leads to a definite improvement of the sensitivity and therefore only a few hundred milligrams of catalyst are used for each experiment. The apparatus and experimental procedure have been described elsewhere (*21*).

b. CO Chemisorption

The amount of CO irreversibly fixed on Pt at 15°C has been determined by gravimetry. Apparatus and experimental procedure have been already described (*21*). The infrared spectra of CO adsorbed on Pt supported on amorphous alumina have shown that CO molecules are linearly bonded to the Pt atom (Pt=C=O, characteristic band at 2070 cm^{-1}) (*21*). These results agree with the conclusions of Blyholder and Sheets (*22*), Lin, Witt and Hammaker (*23*) and Dorling and Moss (*16*). We have therefore assumed that each Pt surface atom of the catalyst irreversibly retains one CO molecule.

For both H_2 and CO chemisorption, the metal surface area, S_{metal} (m^2/g Pt) is derived from the figure of 1.12×10^{19} surface atoms per m^2 of Pt surface (*24*). The mean diameter $\bar{D}_S$ is evaluated from the formula $\bar{D}_S = 6/\rho S$, valid for spherical particles (ρ: density of Pt). This last assumption is based on electron micrographs which show that Pt particles are nearly spherical.

Physical Methods

These methods yield simultaneously the metal surface area and the granulometry laws (*25*). Various types of laws, called particle distribution functions, can be obtained. The first of them is the frequency law, in which the frequency is proportional to the number of particles whose diameters range between two limits. This function, $f_N(D)$, leads to a mean diameter:

$$\bar{D}_N = \int_0^{D_{max}} D \cdot f_N(D) dD.$$

This value is evaluated from the microscopy data by the well-known expression:

$$\bar{D}_N = \frac{\Sigma ND^2}{\Sigma ND}.$$

Likewise, a surface law, $f_S(D)$ and a volume law, $f_V(D)$, can be defined with the corresponding mean diameters:

$$\bar{D}_S = \int_0^{D_{max}} Df_S(D) dD = \frac{\Sigma ND^3}{\Sigma ND^2};$$

$$\bar{D}_V = \int_0^{D_{max}} Df_V(D) dD = \frac{\Sigma ND^4}{\Sigma ND^3}$$

The important point is that all these functions are normalized by the expression:

$$\int_0^{D_{max}} f(D)dD = 1.$$

This procedure is only valid if all the particles have the same shape. When this condition is not fulfilled, the difficulty is solved by choosing for the particle diameter a diameter which is that of an equivalent sphere (a sphere which has the same volume). Actually, all our supported catalysts show nearly spherical particles, even at 800°C.

a. Electron Microscopy

Electron micrographs were taken with a JEM 100 B microscope which permitted a resolution to about 3 Å. Specimen preparation was the same as outlined in (*26*), using the extractive method on carbon films. For each sample, 1000 to 2000 particles were measured, on randomly selected photographs. The direct magnification is 150,000 to 200,000 and the total magnification, on the photographs, 600,000.

b. Small Angle X-Ray Scattering

The experiments were performed on a special small angle goniometer (*27*), fitted with a Guinier type collimation system, which includes a fine focus tube (0.1 mm), a bent quartz monochromator, four slits, a scintillation detector and electronic step scanning. The beam is focused on the detector slit and its dimensions are 0.15 × 25 mm. Such a beam is considered as "infinitely high." The complete intensity curves are registered for values of $s = 2\theta/\lambda$ varying from zero to 8×10^{-1} Å^{-1}, where 2θ is the scattering angle and λ the copper or molybdenum $K\alpha$ wavelength.

At large angles, beyond 2×10^{-2} Å^{-1}, the Porod law is generally followed and the product $I \times s^3$ (in the case of an "infinitely high" beam) tends to its constant asymptotic value. Actually, the curve $I \times s^3$ versus s^3 is a straight line with a slope depending on the value of the background; the intensity then reads: $I(s) = A/s^3 + B$, where B is the background term due to the Laue scattering of the pore maskant, to the counter noise and to incoherent scattering. This background is subtracted from the experimental data to obtain the true scattered intensity. The multiple scattering treatment is then performed on this scattered curve leading to the projection $q(t)$ of the Patterson function on the observation plane and to the function itself, $P(r)$ (*28, 29*). All the parameters available from small angle data can then be computed from $P(r)$ or from $q(t)$: surface area, porosity, various mean diameters and particle distribution functions.

Surface area. The specific area is proportional to the first derivative of the Patterson function at the origin: $S = 4 \times 10^4 [P'(0)/\mu^2]$ where μ is the crystallographic density, $P'(0)$ is calculated from the $P(r)$ function or directly from the asymptotic value of $I \times s^3$. In the present case of an "infinitely high" beam, the expression of $P'(0)$ reads $P'(0) = 16\ \pi^2[\lim\ (I \times s^3)/m\ \nu\ a]$, in which $\nu = 0.00716\ \lambda^2$, λ the wavelength (Å), m the mass of sample in the sample holder (g cm^{-2}), and a the transmitted flux. Generally these two values of $P'(0)$ agree within less than 1%. A first measurement is performed on the support, leading to a value $P'_1(0)$. A second measurement, on the catalyst itself, gives $P'_2(0)$; the area of the metal then reads:

$$S = 4 \times 10^4 \frac{P'_2(0) - P'_1(0)}{\mu^2}.$$

Assuming that the contact area between metal and carrier is low, μ is approximately the density of the metal. One must note that, with platinum, the error due to this approximation is low.

Porosity, mean diameters. The porosity of the support, α, reads

$$\alpha = \frac{(P0)}{\mu^2}.$$

Besides the Guinier radius of gyration, various mean diameters can be calculated. Two of them are specially important since they permit a comparison with electron microscopy results. If we assume that the particles are approximately spherical, Soule (*30*) has shown that the expressions for $\bar{D}_V$ and $\bar{D}_S$ are:

$$\bar{D}_V = K\frac{q(0)}{P(0)} \text{ and } \bar{D}_S = K\frac{P(0)}{P'(0)},$$

where K is a constant.

Particle diameter distributions. The first type of distribution, which involves no assumption on the shape of the particles, is called cord length distribution, $\phi(l)$. This function is the probability that a segment of length l has both extremeties on the particle surface. However, as the physical meaning of this function is not very clear, we prefer to calculate the diameter distribution function with the assumption of a spherical shape. The expression of the volume function $f_V(D)$ is:

$$f_V(D) = K\frac{D^3}{3}\frac{d}{dD}\left(\frac{P''(D)}{D}\right),$$

where $P''(D)$ is the second derivative of the Patterson function and K the normalization constant. This function can also be obtained directly by Fourier-Bessel transformation of the scattered intensity (*28*). Now the question arises of the meaning of this function when the shape of particles is not spherical: it has been shown that in the case of needles or of elongated ellipsoids, it represents the distribution of the diameters of the particle cross-section.

Experimental procedure. A registration of the direct beam is first done. Then, three experiments are performed: (i) on the support treated under the same conditions as the catalyst, (ii) on the evacuated catalyst, (iii) on the catalyst after adsorption of a "pore maskant." In the present case, the pore maskant is CH_2I_2, which has nearly the same electron density as alumina (*31*). This adsorption is conducted in two different ways, either by cooling the outgassed sample at liquid nitrogen temperature and condensing pure CH_2I_2 on it, or by introducing CH_2I_2 dissolved in ether directly to the outgassed sample. A precise control of the amount of CH_2I_2 is necessary; it has to be slightly greater than the pore volume of the support (0.2 $cm^3\ g^{-1}$). However, a large excess of pore maskant leads to a considerable increase in the background. The experiments on this "masked" sample lead to the particle distribution function. The scattering curve obtained from the "unmasked" catalyst gives, by a comparison with the support, the specific area of the metal.

TABLE 1
H_2 CHEMISORPTION; EFFECT OF THE METAL CONTENT[a]

Pt content (%)	H/Pt	S_{metal} (m^2/g Pt)	$\bar{D}_S$ (Å)
	III M Carrier		
0.6	0.84	231	12
1	0.78	215	13
2	0.59	163	17
2.8	0.44	120	23
3.8	0.38	105	27
	IV N Carrier		
0.6	0.88	243	12
1	0.80	221	13
2	0.62	171	16
2.7	0.49	135	21
3.7	0.38	105	27
4.8	0.33	92	30

[a] Reduction temperature: 500°C.

RESULTS AND DISCUSSION

H_2 and CO Chemisorption

The results obtained from H_2 chemisorption, related to two different sets of catalysts prepared from two different amorphous alumina lots (i.e., III M: 137 m^2/g and IV N: 131 m^2/g) containing various amounts of Pt and reduced at 500°C, are shown in Table 1 (*21*). It appears from

TABLE 2
H_2 CHEMISORPTION; EFFECT OF HEAT TREATMENT ON THE 3.7% (IV N) Pt CATALYST

Heat treatment temp (°C)	H/Pt	S_{metal} (m^2/g Pt)	$\bar{D}_S$ (Å)
500[a]	0.38	105	27
600[b]	0.33	89	31
700[b]	0.26	71	39
800[b]	0.26	71	39

[a] Under H_2.
[b] Under H_2 at 500°C and then *in vacuo*.

TABLE 3
CO CHEMISORPTION; EFFECT OF THE Pt CONTENT[a]

Pt content (%)	CO/Pt	S_{metal} (m^2/g Pt)	$\bar{D}_S$ (Å)
0.6	0.79	218	13
1	0.72	199	14
2	0.57	156	18
2.7	0.46	126	22
3.7	0.36	98	29
4.8	0.32	87	32

[a] IV N Carrier reduction temperature: 500°C.

Table 1 that the results are fairly well reproducible.

Table 2 gives the H_2 chemisorption results concerning the heat treatment on a nominal 3.7% (IV N) Pt catalyst. The reduced samples were heated in vacuum, respectively, at 600, 700 and 800°C for 6 hr. The same catalyst (3.7% Pt) heated before reduction, in air at 700°C for 4 hr and then reduced at 600°C for 3 hr, leads to a value of $S = 11$ m^2/g and $\bar{D}_S = 250$ Å (not reported in Table 2).

Table 3 shows the results obtained from CO chemisorption on the IV N Pt catalysts. A comparison of Table 3 (CO results) with Table 1 (H_2 results) shows that both methods lead to the same value of the metal dispersion within a range of 10% (*21*).

Electron Microscopy

The micrographs of the 0.6, 2.0 and 3.7% (IV N) Pt catalysts, reduced at 500°C for 3 hr, are respectively reported in Figs. 1, 2 and 3. Figure 4 is related to the 3.7% (IV N) Pt catalyst, first reduced at 500°C and then heated in vacuum at 700°C for 6 hr. The total magnification is 600,000. Figure 1 shows almost all very fine particles (10–20 Å) with very few 40 Å particles. This micrograph corresponds to the distribution curve in Fig. 5. In Fig. 2, more 40–50 Å particles appear as can be seen in the distribution curve of Fig. 6. The situation is more delicate with the reduced 3.7% sample: half of the volume is composed of 40–50 Å particles which correspond to only 5% of the total number of particles. Therefore, a small "sampling error" in selecting the micrographs had led to an important perturbation in the distribution curve (Fig. 7). The situation is still worse when this catalyst (3.7% IV N Pt) is heated, after reduction, at 700 or 800°C in vacuum (Figs. 4 and 8, curve 3). All the diameters between 15 and 150 Å are present in the sample and it is difficult to make sure whether some large clusters are composed of several fine particles or not. Moreover, it is almost impossible to obtain a correct distribution curve, since 2 or 3% of the total number of particles have a diameter comprised between 80 and 150 Å but they can easily contribute 50% of the volume. The statistical error being high on such a sample, the resulting error in the distribution curve can reach 20 to 30%.

Table 4 summarizes the electron microscopy results obtained from IV N Pt catalysts containing increasing Pt content.

Small Angle X-Ray Scattering

As expected, the Porod law is followed at very high values of s, above $s = 0.5 \times 10^{-1}$ Å^{-1}. This fact is, of course, due to the very small size of the metal particles. Therefore, after subtraction of the continuous background, a precise evaluation of the Porod invariant is possible in the zone $0.5\text{–}0.8 \times 10^{-1}$ Å^{-1}. The plot of $I(s)s^3$ versus s is shown in Fig. 9 where curves 1 and 3 show the experimental data concerning, respectively, the 3.7% catalyst and the carrier. In curve 2, are plotted values of curve 1 after correction for the continuous background (see experimental section). Of

TABLE 4
ELECTRON MICROSCOPY[a]

Pt content (%)	$\bar{D}_v$ (Å)	$\bar{D}_s$ (Å)	S_{metal} (m^2/g Pt)
0.6	23	16	175
2	29	18	155
3.7	38	24	116

[a] IV N Pt catalysts; reduction temperature: 500°C.

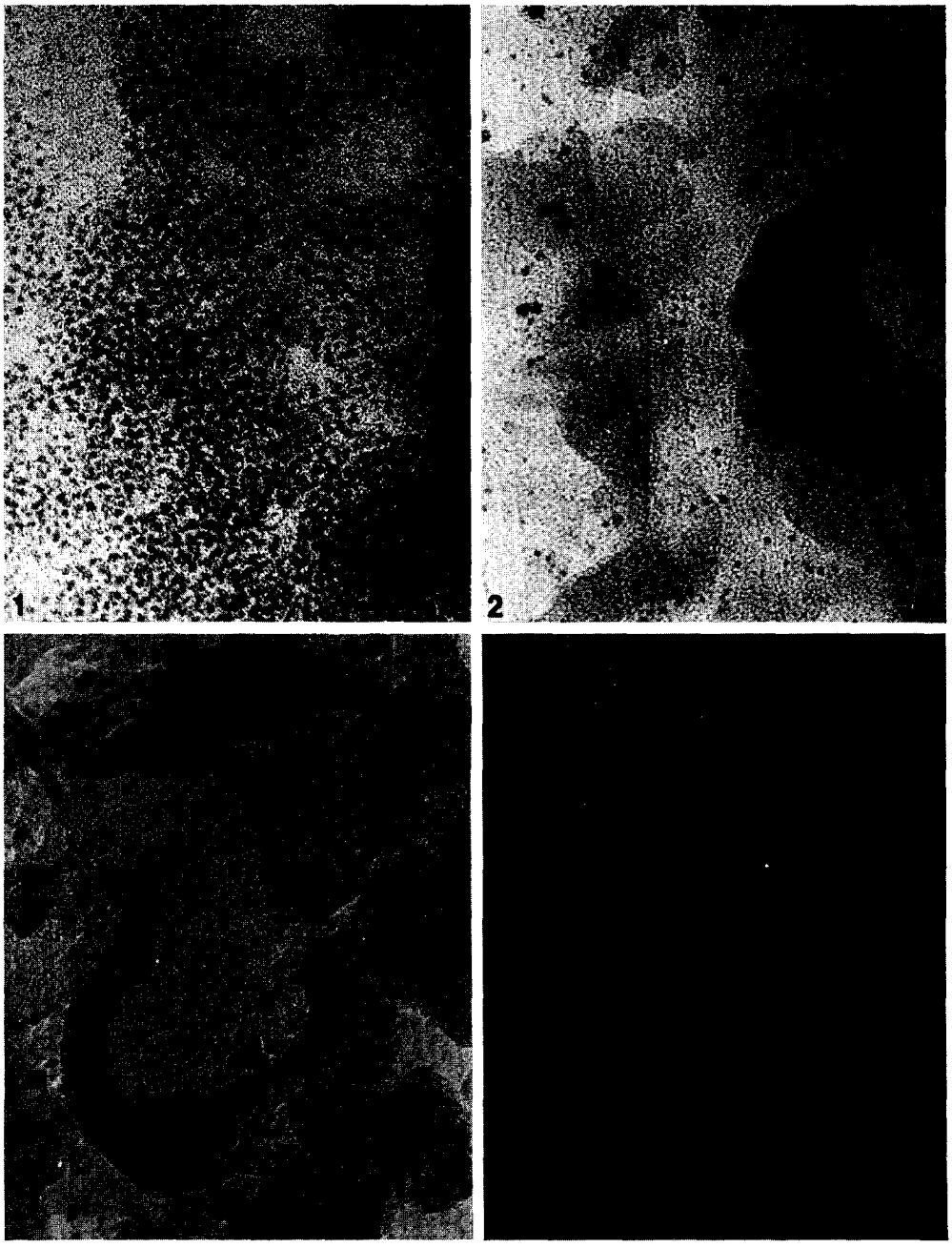

FIG. 1. Electron micrograph of the 0.6% Pt (IV N) catalyst; ×600,000.
FIG. 2. Electron micrograph of the 2% Pt (IV N) catalyst; ×600,000.
FIG. 3. Electron micrograph of the 3.7% Pt (IV N) catalyst; ×600,000.
FIG. 4. Electron micrograph of the 3.7% Pt (IV N) catalyst, after treatment in vacuum at 700°C; ×600,000.

course, the larger the amount of Pt, the larger the difference between the value of $P'(0)$ for the catalyst and the carrier, and the smaller the error in evaluation of the area. It can be seen in Table 5 (see below) that this difference is 25% in the case of the 0.6% catalyst and 100% in the case of the 4.3% catalyst.

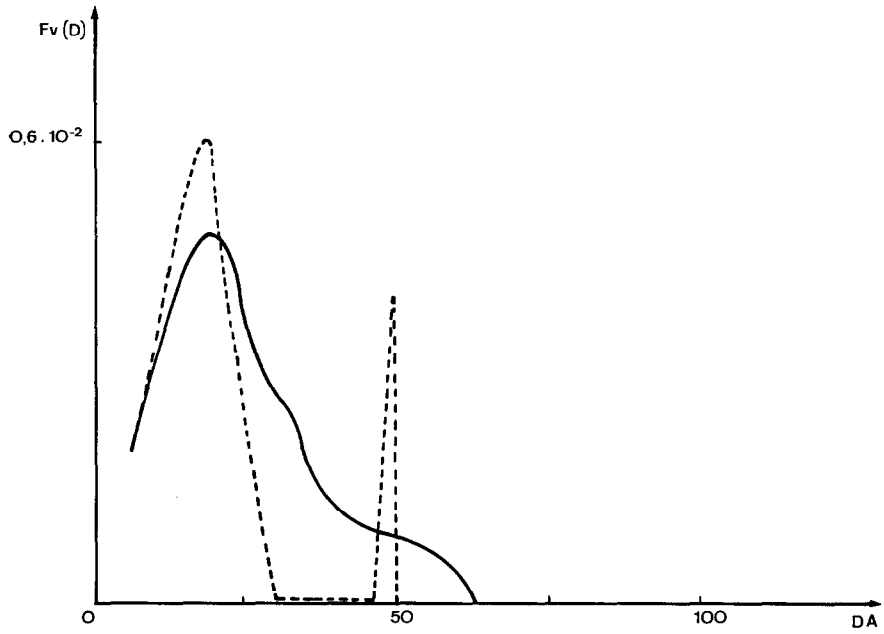

FIG. 5. Distribution of metal particle diameters of the 0.6% Pt (IV N) catalyst. (- - -) Electron microscopy; (—) SAXS.

a. Effect of Pt Content

Table 5 shows the effect of the Pt content on parameters measured by small angle scattering. The $\bar{D}_v$ and $\bar{D}_s$ diameters rapidly increase when the amount of Pt is increased from 0.6 to 2%. For larger Pt contents, the increase is slower. In the curves shown in Figs. 5, 6 and 7 (for 0.6, 2 and 3.7% samples) the particle diameters are plotted as a function of their volume

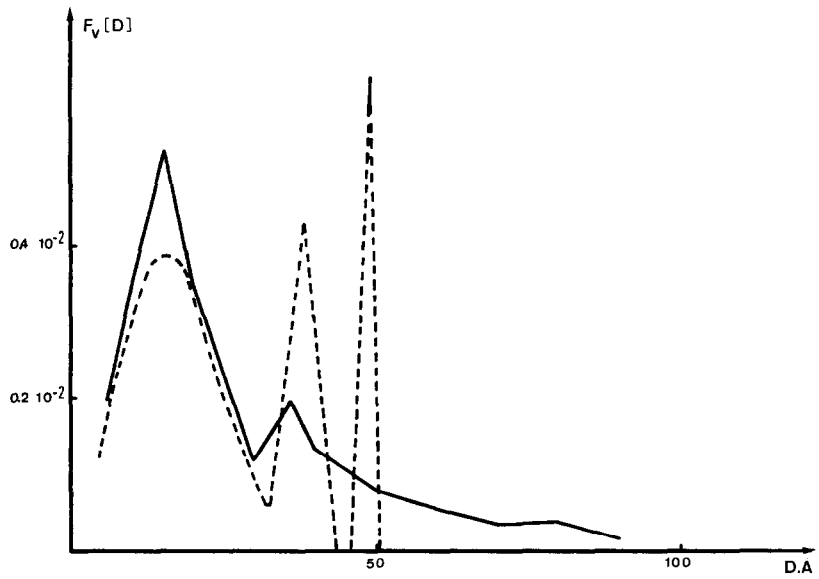

FIG. 6. Distribution of metal particle diameters of the 2% Pt (IV N) catalyst. (- - -) Electron microscopy; (—) SAXS.

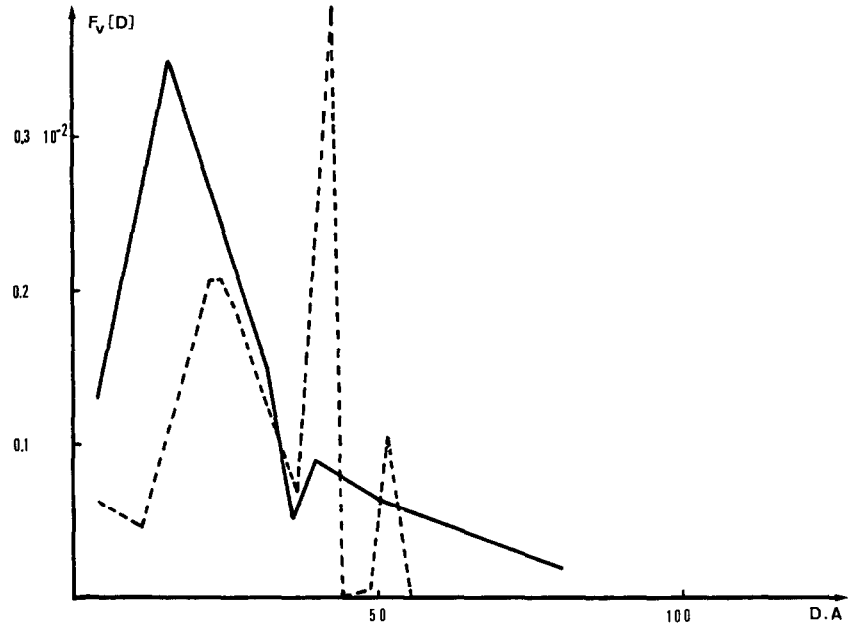

FIG. 7. Distribution of metal particle diameters of the 3.7% Pt (IV N) catalyst. (- - -) Electron microscopy; —) SAXS.

fraction. A very slight shift of the main maximum (D_{max}) occurs (see Table 5, last column), when the concentration of Pt is increased from 0.6 to 4.3%, while the $\bar{D}_v$ diameter is multiplied by 2.5. In the distribution curve corresponding to the 0.6% sample (Fig. 5), there is only one maximum located at 15 Å, followed by an

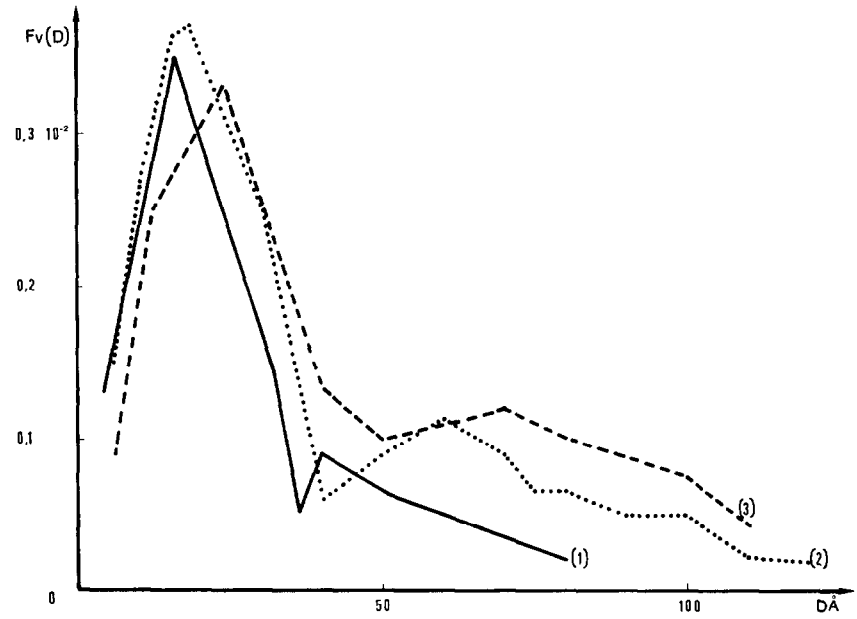

FIG. 8. SAXS distribution of metal particle diameters of the 3.7% Pt (IV N) catalyst. (1) Only reduced at 500°C; (2) reduction at 500°C + heat treatment in vacuum at 600°C; (3) reduction at 500°C + heat treatment in vacuum at 700 or 800°C.

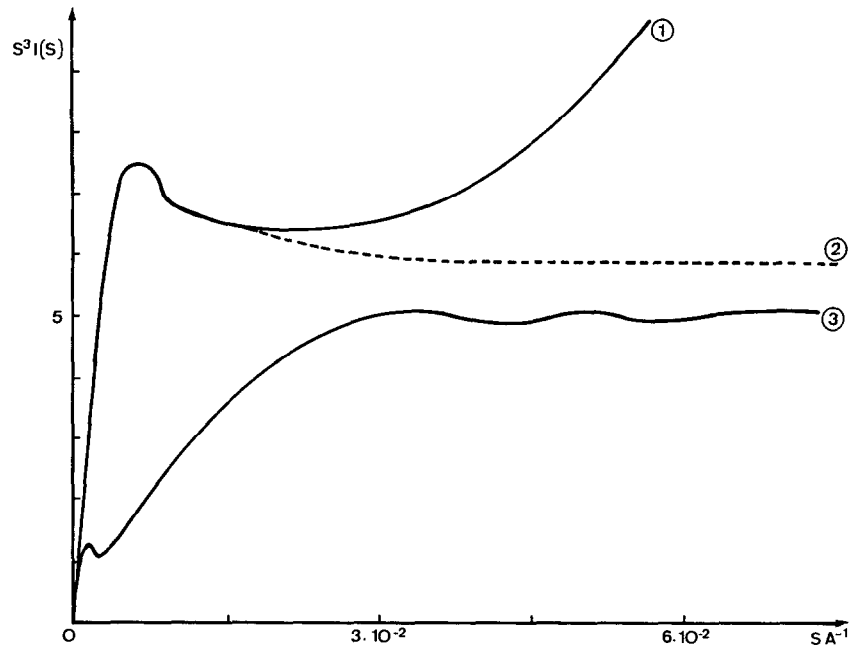

FIG. 9. $I(s)s^3$ vs s: (1) Rough data, 3.7% Pt (IV N) catalyst; (2) corrected for continuous background, 3.7% Pt (IV N) catalyst; (3) rough data, carrier.

oscillating tail with a slight bump at 30 Å. When the Pt concentration reaches 2% (Fig. 6), a broadening of the peak at 15 Å is observed and a true maximum appears at 30 Å. At first sight, this slight difference between the two curves does not account for a difference of 40% in the metal areas. This contradiction is probably due to our measuring procedure, since the pore maskant (CH_2I_2) only fills about 80% of the porosity and in the case of the 0.6% sample, the tail of the curve is precisely in the range of abscissae of these unfilled pores, i.e., 30–60 Å, as shown in Fig. 10, where the pore diameter distribution of the carrier is plotted. In the case of the 3.7% sample, there are simultaneously an increase in the size of metal particles (40 Å) and a considerable augmentation of the volume fraction of these large particles (Fig. 7).

TABLE 5
SMALL ANGLE X-RAY SCATTERING (IV N CARRIER); EFFECT OF THE METAL CONTENT ON THE CATALYSTS REDUCED AT 500°C

Pt content (%)	$P'(0)$ (g cm^{-3} Å^{-1})	S_{metal} (m^2/g Pt)	$\bar{D}_S$ (Å)	$\bar{D}_v$ (Å)	D_{max}[a] (Å)
0	430	140[b]			
0.6	590	225	13	22	15
2	670	126	22	38	15
3.7	830	105	28	45	16
4.3	860	95	32	55	

[a] D_{max} is the abscissa of the maximum of the distribution curve.
[b] S support (m^2/g Al_2O_3).

So, when the amount of Pt is increased from 0.6 to 4% the size of the finest particles remains nearly constant, but there is a large increase in the volume fraction of large particles (30–80 Å).

b. Effect of the Heat Treatment

The results concerning the heat treatment of the 3.7% Pt (IV N) catalyst are illustrated in Fig. 8 and summarized in Table 6. Samples are first reduced at 500°C and then heated in vacuum, respectively, at 600, 700 and 800°C for 6 hr. It can be seen that the sintering of the metal mainly occurs between 600 and 700°C (Table 6). In Fig. 8, it appears that the main maximum is progressively shifted from 16 to

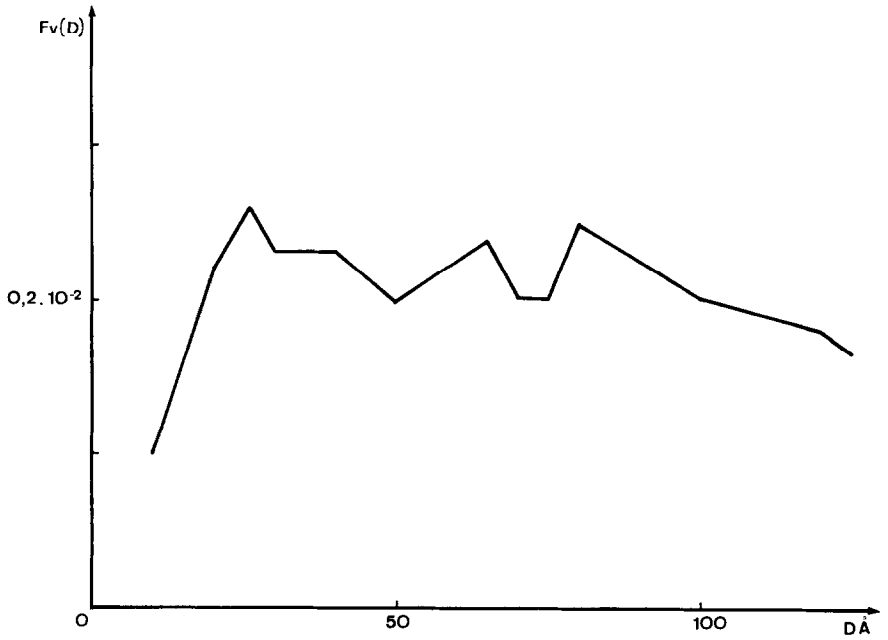

FIG. 10. SAXS distribution of pore diameters of the carrier.

25 Å and the secondary peak from 40 to 75 Å. In fact, it is probable that some very large particles (300–400 Å) are formed which increase strongly the mean diameters.

The results obtained from the four techniques are gathered in Table 7. We have seen that each technique leads to self-consistent results; the metal area (m^2/g Pt) decreases with Pt content and with temperature increase. However, a significant difference appears from this comparison, especially when the dispersion is not very good. For the 0.6% sample, all the methods agree on the value of the metal area and on the diameter of particles. The dispersion of the metal is very good for this sample and the distribution curves of the diameter very narrow, showing a maximum at 15 Å. In the case of the 2% sample, the agreement is still good. X-Ray and electron microscopy show that 20% of the volume is composed of particles with diameter ranging between 25 and 50 Å. For the 3.7% sample, half of volume of the metal is composed of particles with a diameter less than 30 Å and both distribution curves (X-ray and electron microscopy) show an oscillating tail reaching 100 Å. In that case, the metal area is the best parameter for characterizing the sample. The situation is more critical for the samples (3.7% Pt) heated at 700 or 800°C. Their distribution curves are broad (Fig. 8, curve 3), as expected from the large difference between $\bar{D}_v$ and $\bar{D}_s$ values (Table 7). In that case, the results obtained by electron microscopy are not reliable, since it is difficult to select a number of micrographs which really represent the sample. However, for these catalysts, the X-ray distribution curves seem to be more reliable, as metal areas obtained from X-ray and adsorption methods are in good agreement (about 60 and 70 m^2/g Pt, Table 7).

TABLE 6

SMALL ANGLE X-RAY SCATTERING; EFFECT OF THE HEAT TREATMENT ON THE 3.7% Pt (IV N) CATALYST

Temp (°C)	S_{metal} (m^2/g Pt)	$\bar{D}_S$ (Å)	$\bar{D}_v$ (Å)	D_{max} (Å)
500[a]	105	27	45	16
600[b]	95	30	50	18
700[b]	60	45	70	25
800[b]	58	46	80	25

[a] Under H_2.

[b] Under H_2 at 500°C and then *in vacuo*.

TABLE 7
COMPARISON OF THE RESULTS[a]

Sample		Metal area (m^2/g Pt)				Diameter (Å)							
						Adsorption		X-Rays			Electron microscopy		
Pt content (%)	Treatment temp (°C)	H_2	CO	X-Ray	EM	(H_2) ($\bar{D}_S$)	CO ($\bar{D}_S$)	$\bar{D}_S$	$\bar{D}_v$	D_{max}	$\bar{D}_S$	$\bar{D}_v$	D_{max}
0.6	500[b]	243	218	225	180	12	13	13	22	15	16	23	15
1	500[b]	221	199			13	14						
2	500[b]	171	156	125	166	16	18	22	38	15	18	29	15
2.7	500[b]	135	126			21	22						
3.7	500[b]	105	98	105	125	27	29	27	45	16	24	38	25
4.8	500[b]	92	87	90		30	32	32	55				
3.7	600[c]	89		95	130	31		30	50	18	23	33	
3.7	700[c]	71		60	91	39		44	70	25	33	51	25
3.7	800[c]	71		58	56	39		46	80	25	53	95	100

[a] IV N carrier.
[b] Under H_2.
[c] Under H_2 at 500°C and then *in vacuo*.

An interesting point arises from the difference of metal area measured by hydrogen and CO chemisorption or small angle X-ray scattering. This difference is approximately 10% and several explanations can be put forward:

i. This difference is not significant; it is caused by the difference in the experimental procedures applied to chromatography and gravimetry techniques. However, it must be mentioned that H_2 results always give areas greater than CO results (Table 7).

ii. As reported by several authors (*16*), a few percent of CO molecules are "bridge-bonded." In that case, the H_2 values would be more exact. However, the X-ray results, close to those of CO, are difficult to explain, since they are also absolute measurements, free from any assumption about particle shape.

iii. This difference corresponds to the area of contact between metal and carrier. Actually, it is reasonable to assume that hydrogen can diffuse over this area while CO molecules cannot.

The third explanation seems to be the best, since it agrees well with X-ray data: $P'(0)$, from which area is derived, is in that case underestimated, as the transition in electron density is taken equal to $\rho_{Pt} - \rho_{air}$. So, the total metal area could be measured by hydrogen chemisorption, while the accessible area could be measured by CO chemisorption and small angle X-ray scattering.

CONCLUSIONS

The present work has shown that, for the most diluted catalyst (up to 2% Pt), where metal is finely dispersed and the distribution curves merely present one sharp maximum, the results obtained from chemisorption techniques, small angle X-ray scattering and electron microscopy lead to practically identical conclusions. However, when the metal dispersion is less good, the distribution curves obtained by X-rays remains a satisfying representation of the reality, while the values obtained by electron microscopy are less reproducible. In that case, the most reliable parameter is the metal area measured by X-rays or chemisorption.

On the other hand, the agreement in the values of metal area obtained by X-rays and chemisorption is good enough to confirm our hypothesis on the stoichiometry of the chemisorption of H_2 and CO on Pt catalysts. Moreover, there is no modification of this stoichiometry with Pt particle size, even for ultrafine particles.

Finally, from the economic standpoint, our results related to the effect of Pt content outline the unprofitability of exceeding the content of about 1% of Pt, since any higher metal excess is incorporated in bigger particles which should be of considerably less catalytic efficiency.

ACKNOWLEDGMENTS

The authors gratefully acknowledge the E.M. Service of the I.R.C. for producing electron micrographs and giving helpful advice. Professors Imelik and Teichner are thanked for fruitful discussions.

REFERENCES

1. HOANG-VAN, C., AND TEICHNER, S. J., *Bull. Soc. Chim. Fr.* 1498 (1969).
2. HOANG-VAN, C., JUILLET, F., AND TEICHNER, S. J., *Bull. Soc. Chim. Fr.* 1504 (1969).
3. HOANG-VAN, C., AND TEICHNER, S. J., *J. Catal.* **16,** 69 and 75 (1970).
4. HOANG-VAN, C., GHORBEL, A., AND TEICHNER, S. J., *Buil. Soc. Chim. Fr.* 437 (1972).
5. HOANG-VAN, C., COMPAGNON, P. A., AND TEICHNER, S. J., *Bull. Soc. Chim. Fr.*, in press; COMPAGNON, P. A., thesis, Lyon, 1973.
6. BUSSIÈRE, P., LAURENT, A., AND JUNOD, E., *J. Radio. Anal. Chem.* **2,** 211 (1969).
7. GIL'DEBRAND, E. I., *Int. Chem. Eng.* **6,** 449 (1966).
8. SINFELT, J. H., *Chem. Eng. Progr. Symp. Ser.* **63,** 16 (1967).
9. BOUDART, M., *in* "Advances in Catalysis" (D. D. Eley, H. Pines and P. B. Weisz, Eds.), Vol. 20, p. 153. Academic Press, New York, 1969.
10. MULLER, J., *Rev. Pure Appl. Chem.* **19,** 151 (1969).
11. BOND, G. C., *Surface Sci.* **18,** 11 (1969).
12. MEARS, D. E., AND HANSFORD, R. C., *J. Catal.* **9,** 125 (1967).
13. ZAIDMAN, N. M., DZISKO, V. A., KARNAUKHOV, A. P., KRASILENKO, N. P., AND KOROLEVA, N. G., *Kinet. Katal.* **10,** 652 (1969).
14. KARNAUKHOV, A. P., *Kinet. Katal.* **12,** 1520 (1971).
15. WILSON, G. R., AND HALL, W. K., *J. Catal.* **17,** 190 (1970).
16. DORLING, T. A., AND MOSS, R. L., *J. Catal.* **7,** 378 (1967).
17. GRUBER, H. L., *Anal. Chem.* **34,** 1828 (1962); *J. Phys. Chem.* **66,** 48 (1962).
18. BENSON, J. E., AND BOUDART, M., *J. Catal.* **4,** 704 (1965).
19. GERMAIN, J. E., OSTYN, M., AND BEAUFILS, J. P., *J. Chim. Phys.* **61,** 686 (1964).
20. FIGUERAS, F., DE MOURGUES, L., AND TRAMBOUZE, Y., *J. Gas Chromatogr.* **6,** 161 (1968).
21. COMPAGNON, P. A., HOANG-VAN, C., AND TEICHNER, S. J., *Bull. Soc. Chim. Fr.*, in press; COMPAGNON, P. A., thesis, Lyon, 1973.
22. BLYHOLDER, G., AND SHEETS, R., *J. Phys. Chem.* **74,** 4335 (1970).
23. LIN, K. C., WITT, J. D., AND HAMMAKER, R. M., *J. Chem. Phys.* **55,** 1148 (1971).
24. SPENADEL, L., AND BOUDART, M., *J. Phys. Chem.* **64,** 204 (1960).
25. MARTIN, G., MORAWECK, B., RENOUPREZ, A., DALMAI, G., AND IMELIK, B., *J. Chim. Phys.* **3,** 532 (1972).
26. ÉLINARD, C., AND OBERLIN, A., *J. Microsc. (Paris)* **10,** 215 (1971).
27. RENOUPREZ, A., BOTTAZZI, H., WEIGEL, D., AND IMELIK, B., *J. Chim. Phys.* **62,** 131 (1965).
28. BRUSSET, H., AND DONATI, J. R., *J. Appl. Crystallogr.* **2,** 55 (1969).
29. RENOUPREZ, A., IMELIK, B., *J. Appl. Crystallogr.* **6,** 105 (1973).
30. SOULE, J. L., *J. Phys. Radium.* **18,** 90 A (1957).
31. WHYTE, T. E., KIRKLIN, P. W., GOULD, R. W., AND HEINEMANN, H., *J. Catal.* **25,** 407 (1972).